Atom Indonesia

Journal homepage: http://atomindonesia.brin.go.id

The Modelling and Analysis of iPWR-Type SMR Core Dynamics: Control Rods, Reactivity Feedback, and Thermal-Hydraulic Effects

G. Septawijaya[1*], S. Sukarman[1], S. Bakhri[2], M. Subekti[3]

[1]*Electronics and Instrumentation Department, Polytechnic Institute of Nuclear Technology, Yogyakarta 55281, Indonesia*
[2]*Research Centre for Nuclear Fuel Technology and Radioactive Waste, National Research and Innovation Agency, South Tangerang 15310, Indonesia*
[3]*Directorate for Nuclear Facility Management, National Research and Innovation Agency, Central Jakarta 10340, Indonesia*

ARTICLE INFO

Article history:
Received 8 January 2024
Received in revised form 9 July 2024
Accepted 18 July 2024

Keywords:

Neutronic
Thermal hydraulic
Small Modular Reactor core

ABSTRACT

Development plans for Nuclear Power Plants (NPPs) in Indonesia have been widely discussed. One of the planned NPP types is the Small Modular Reactor (SMR). Human resource readiness is an essential aspect to be considered before constructing an NPP. Simulators capable of illustrating core dynamics can be used to educate the public about the processes within a nuclear reactor. Core modeling is a key component in developing an NPP simulator. The neutronic behavior of the reactor core is modeled using point kinetics equations, while the thermal-hydraulic aspect uses Mann's model. The results indicate that the modeled core can operate up to 160 MWt and other operating parameters at maximum power align well with the SMR reactor design certification data.

INTRODUCTION

In February 2014, the Indonesian government issued the National Energy Policy, which includes nuclear energy as one of the new energy sources. As part of its commitment to reducing emissions, the Indonesian government has set a road map to achieve Net Zero Emissions by 2060. According to this road map, nuclear power plants will be integrated into Indonesia's power generation system starting in 2032 [1,2].

An integral Pressurized Water Reactor (iPWR) is a reactor design where the primary cooling system's main components, such as the steam generator, pressurizer, and Control Rod Drive Mechanism (CRDM), are located within a single reactor pressure vessel (RPV). This innovative design offers natural circulation as one of the passive safety systems and eliminates several potential accident initiators [3,4].

In recent years, many iPWR-type Small Modular Reactors (SMRs) have been developed. These SMRs are particularly notable for their modular nature, allowing for the construction of small, self-contained nuclear units that can be deployed individually or in clusters, providing a flexible and scalable solution for power generation. Their passive safety systems and compact design enhance safety standards, making them a compelling candidate for the future of clean and sustainable energy production [3].

SMRs present a viable alternative to reduce the Outer Java-Bali region's dependence on oil-based power plants. Furthermore, a probabilistic approach used in a previous study concluded that there is a 20 % probability of rejecting the SMR project, indicating an 80 % likelihood of its feasibility. Given the significant potential for SMR development in Indonesia, it is necessary to prepare human resources [5].

Simulators are essential in education, serving as effective tools for disseminating information to both the public and students. There are two types of simulators: basic education and training simulators, which illustrate general concepts, and demonstrate fundamental physical processes in a nuclear power plant, and professional training simulators, which represent plant components, systems, and their functions, Professional simulators provide detailed

*Corresponding author.
E-mail address: gilang.septawijaya11@gmail.com
DOI: https://doi.org/10.55981/aij.2024.1414

insight into the comprehensive operation of a specific NPP, simulating normal, transient, and accident conditions, and showing the internal effects on various system parameters [6].

Most existing SMR simulators are proprietary and specific to particular vendors and commercial reactors. Although the International Atomic Energy Agency (IAEA) has developed a generic SMR simulator, its further development is limited [7]. Additionally, there are currently no universities or industries in Indonesia actively involved in simulator development before the construction of nuclear power plants. Based on these issues, the main objective of this paper is to propose an SMR reactor core model that demonstrates the integration of neutronic and thermal-hydraulic models using LabVIEW, providing a reference for future SMR simulator development in Indonesia.

In previous studies, Ardiansyah and Oktavian evaluated a two-stage diffusion approach for IPWR core analysis, combining the Monte Carlo code Serpent for reference and the diffusion code PARCS for cost-efficient simulations. The method accurately determined the neutron multiplication factor and core power distribution but requires further refinement for improved precision [8]. Meanwhile, Blackett assessed aspects such as the simulator control room layout, alarm system capabilities, and human-machine interface (HMI) to identify the simulator's limitations and potential areas for future research [9]. In addition, this paper proposes new equation combinations for modeling the reactor core, particularly in LabVIEW software. Thus, selecting the appropriate model or approach is pivotal in the simulator development process.

Point kinetics is a simplified method for modeling the neutron dynamics of a nuclear reactor [10]. It assumes that the neutron flux distribution is reduced to a single point, with reactor power represented by a single variable. Point kinetics is commonly used to analyze the behavior of reactors during transients and accidents. Fuel temperature is an important parameter that affects the neutron dynamics of a reactor. As fuel temperature increases, neutron moderation decreases, while and Doppler broadening of the neutron absorption resonances increases [11]. Both effects lead to a decrease in the reactivity of the reactor.

The primary focus of this study is to investigate and analyze key aspects of reactor core dynamics during normal operation, including control rod movements, reactivity feedback, and thermal-hydraulic effects. This simulator model can also be easily modified and adapted for specific applications.

METHODOLOGY

REACTOR CORE MODEL

Small modular reactor overview

An SMR module is capable of producing 45 MWe of power. Each nuclear steam supply system, as shown in Fig. 1, is immersed in a pool with dimensions of 6m wide, 6m long, and 23m deep. The main components of the reactor module are the reactor core, steam generator, and pressurizer [12]. This SMR design does not require a coolant pump due to natural circulation in the primary coolant system. The primary coolant is heated as it passes through the reactor core and flows into the hot leg riser. Convection and buoyancy force on the heated coolant can drive the coolant upward. Subsequently, the primary coolant travels downward to the steam generator, where heat is transferred to the secondary coolant. The lower-temperature primary coolant then enters the bottom of the reactor core through the downcomer.

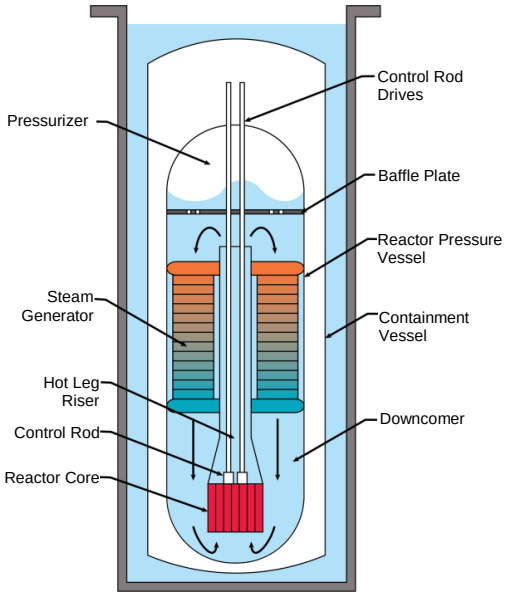

Fig. 1. Schematic of the iPWR-type SMR module [12].

The SMR core design consists of 37 fuel assemblies, each arranged in a 17x17 grid, and consists of 264 fuel rods, 24 control rod guide tubes, and one instrumentation tube at the center of the grid, as shown in Fig. 2. The fuel rods are supported by five spacer grids. Each fuel rod consists of a column of stacked cylindrical ceramic pellets of uranium dioxide (UO_2) enriched with gadolinium oxide (Gd_2O_2), which acts as an absorbent that can be homogeneously burned in the fuel at a selected location. The fuel pellets are encased in zirconium-based alloy cladding, with an active fuel length of 78.74 inches. The fuel is enriched to 4.95 % [13,14]. Table 1 summarizes the SMR core design specifications.

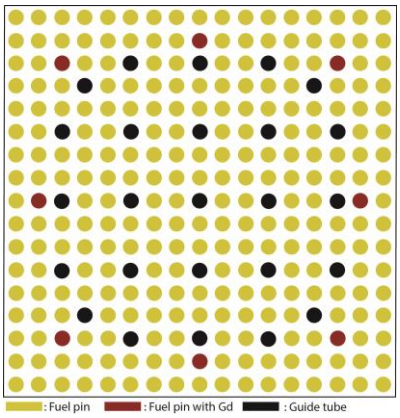

Fig. 2. Small modular reactor fuel grid.

Table 1. Small modular reactor core specification summary.

Parameter	Value
Reactor thermal Power (MWt)	160
Power plant output (MWe)	45
Reactor Pressure (Pa)	12.75
Active core height (m)	2
U-235 enrichment (%)	<4.5
Core inlet temperature (K)	535
Core outlet temperature (K)	592
Heat transfer area on fuel surface (m^2)	583.002
Core flow area (m^2)	0.9095
Average coolant mass flow rate (kg/s)	587.15
Number of the fuel assembly	37

Simulator development

Before starting to build the simulator, the overall design must be defined. Reactor core modeling involves actual operational and physical specification data to ensure that the dynamics are appropriate for the desired reactor type. Figure 3 shows the reactivity feedback mechanism model.

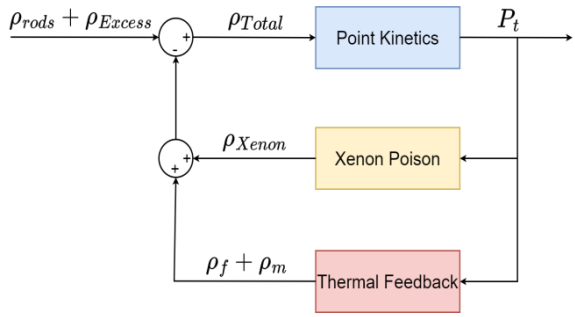

Fig. 3. Reactivity feedback mechanism model.

Afterward, simulator development can be started and is divided into three parts. First, the reactor core is modeled using mathematical equations commonly employed in reactor core simulations, with the difference being the use of iPWR specification data. The second part involves developing the simulator interface using the features available in LabVIEW. The interface is kept simple but capable of displaying all vital parameters for nuclear reactor operation. The final part of simulator development is model verification, ensuring that the created models accurately reflect the actual reactor core design. The simulator structure consists of two main systems: The "simulator-user interaction" system and the "reactor interaction" system manages the buttons and displays that the user can control during simulator operation, while the "reactor core modeling" system contains a core model consisting of neutronic, thermal-hydraulic, and reactivity models.

Point reactor kinetics equation

The point reactor kinetics equation is a differential equation that describes reactor kinetics by modeling the time-dependent changes in the number of neutrons and neutron precursors. This equation is derived by neglecting spatial dependencies and assuming a single neutron energy group. The point kinetic equation is presented in Eq. (1) below [15,16].

$$\frac{dn}{dt} = \left[\frac{\rho(t)-\beta}{\Lambda}\right] n(t) + \sum_{i=1}^{6} \lambda_i C_i(t), \qquad \frac{dC_i}{dt} = \frac{\beta_i}{\Lambda} n(t) - \lambda_i C_i(t), \quad i = 1,\ldots,6 \tag{1}$$

Where, $\Lambda = \frac{l}{k}$ and $\rho = \frac{k-1}{k}$. Eq. (1) above can be solved using an exponential function as shown by the following equation.

$$n(t) = n_0 e^{\omega t}, C_i(t) = C_{i0} e^{\omega t} \tag{2}$$

Then, substituting Eq. (2) and Eq. (1) will result in Eq. (3).

$$\rho = \frac{\omega l}{\omega l + 1} + \frac{1}{\omega l + 1} \sum_{i-1}^{6} \frac{\omega \beta_i}{\omega + \lambda_i} \tag{3}$$

Eq. (3) has 7 roots for the value of ρ $(-\infty \leq \rho \leq 1)$. Thus, the solution of the reactor kinetics equations with delayed neutron is given by Eq. (4).

$$n(t) = \sum_{j=0}^{6} A_j e^{\omega_j t} \tag{4}$$

A_j Coefficient value is shown by Eq. (5) below [15,17,18].

$$A_j = \left(\Lambda + \sum_{i=1}^{6} \frac{\beta_i}{\omega_j + \lambda_j}\right) \Big/ \left(1 + k \sum_{i=1}^{6} \frac{\beta_i}{(\omega_j + \lambda_j)^2}\right) \tag{5}$$

The results of the equation calculation produce the neutron density, which is then used to calculate the reactor period. The reactor period is defined as the amount of time, normally in seconds, required for neutron density (power) to change by a factor of e or 2.718 [19].

$$n(t) = n_0 e^{\frac{t}{T}} \quad (6)$$

Eq. (6) can determine the state of the reactor. When T is negative, the nuclear reactor operates in a subcritical state; When T is zero, the nuclear reactor is in a stable state; when T is positive, the nuclear reactor is in a supercritical state.

It is known that each fission produces 32 pJ of energy, so it takes 3.125×10^{10} fissions per second to produce 1 watt of thermal power. If we assume a reactor with a volume of V_r cm^3, and there will be an average fission of $V_r\Sigma_r\phi$. The reactor power generated from the core fission reaction is given by Eq. (7) below [17].

$$P = \frac{\Sigma_f \phi V_r}{3{,}125 \times 10^{10}} \quad (7)$$

Control rod

The control rod regulates the nuclear fission reaction rate in the reactor. Measuring control rod reactivity is essential for analyzing and assessing shutdown margins in a nuclear reactor [17,20]. The control rod curve model is represented by the following Eq. (8).

$$\rho(z) = \frac{bank_{worth}}{1 + \exp(\frac{z - x_o}{b})} \quad (8)$$

The second term in Eq. (9) ensures that, at full withdrawal, the control rod value becomes zero, and remains negative [21].

$$\rho(z) = \frac{bank_{worth}}{1 + \exp(\frac{z - x_o}{b})} - \frac{bank_{worth}}{1 + \exp(\frac{length - x_o}{b})} \quad (9)$$

Reactivity feedback

The reactivity ($\rho_{net}(t)$) is the sum of the external reactivity ($\rho_{ext}(t)$) applied to the reactor and the feedback reactivity ($\rho_f(t)$) resulting from internal factors within the reactor [15]. The schematic of the feedback mechanism is shown in Fig. 4.

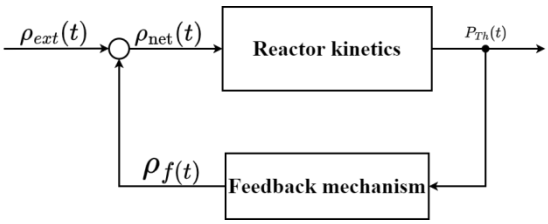

Fig. 4. Feedback reactivity mechanism.

In this model, feedback reactivity is affected by fuel temperature, moderator temperature, and xenon poisoning, while external reactivity is controlled by the control rod. The total reactivity applied to the reactor core is described by Eq. (10).

$$\rho_{total} = \rho_{rod} + \rho_{Xenon} + \rho_f + \rho_m \quad (10)$$

Xenon poison model

The most important fission product poisoning comes from Xe-135, which has a thermal absorption cross-section of 2.7×10^6 barns. This isotope is formed from the decay of I-135 and is also produced directly from the fission of U-235 [22].

Since Xenon is generated from the decay of Iodine, its concentration at any given time depends on the Iodine concentration. The rate of iodine concentration is shown by Eq. (11) below.

$$\frac{dI}{dt} = \gamma_I \Sigma_f \phi - \lambda_I I \quad (11)$$

The Xenon production rate is the sum of xenon produced from iodine decay and U-235 fission, minus xenon that decays and absorbs neutrons, as mathematically represented by Eq. (12) [23].

$$\frac{dX}{dt} = \lambda_I I + \gamma_X \Sigma_f \phi - \lambda_X X - \sigma_{aX} \phi X \quad (12)$$

Thus, the reactivity caused by xenon poisoning is given by Eq. (13) [24].

$$\rho_X = -\frac{\sigma_a^X (X - X_0)}{\Sigma_f} \quad (13)$$

Thermal-hydraulic model

Heat transfer calculation inside fuel element

Heat transfer within the fuel is analogous to an electrical circuit. The temperature difference between the center temperature of the fuel and the outer surface of the fuel element is shown by Eq. (14):

$$T_{max} - T_{fo} = \frac{q'}{4\pi k_f} \quad (14)$$

The temperature drops along the fuel gap is predicted using Eq. (15) below.

$$T_{fo} - T_{ci} = \frac{q'}{2\pi R_g h_g} \quad (15)$$

Meanwhile, the temperature drop between the outer cladding and the inner cladding is determined as follows.

$$T_{ci} - T_{co} = \frac{q'}{2\pi R_c k_c/\delta_c} \quad (16)$$

The temperature of the fuel meat to cladding changes based on the reactor power [25].

Heat transfer from fuel to coolant

The thermodynamics of the reactor core are described using Mann's model, which includes one fuel node and two coolant nodes. In Mann's model, the driving temperature difference is represented by the difference between the fuel temperature, T_F, and the average temperature of the first coolant node, T_{C1}. The output temperature at the second coolant node, T_{C2}, represents the temperature of the coolant exiting the core, as shown in Fig. 5 below [26].

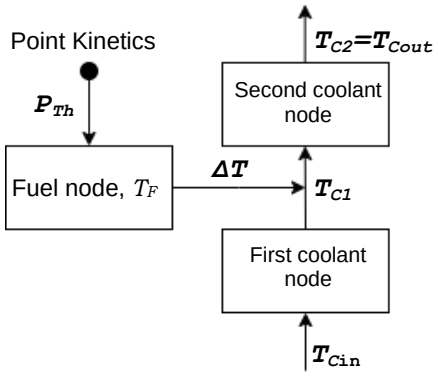

Fig. 5. Heat transfers are nodal on the reactor core.

The above model is based on several assumptions:

- One-dimensional fluid flow.
- The coolant is assumed to be well-stirred.
- The heat transfer coefficient between the fuel and the coolant is constant.

The differential equations for heat transfer from the fuel to the coolant, based on Mann's model and these assumptions, are given by Eqs. (17-19) [27].

$$\frac{d}{dt}\left(m_F c_{p,F} T_F\right) = f_d P - (UA)_{FC}(T_F - T_C) \quad (17)$$

$$\frac{d}{dt}\left(\frac{m_C}{2} c_{p,C} T_{C1}\right) = \frac{1-f_d}{2} P + \left(\frac{UA}{2}\right)_{FC}(T_F - T_{C1}) - \dot{m}_c c_{p,C}(T_{C1} - T_{Ci}) \quad (18)$$

$$\frac{d}{dt}\left(\frac{m_C}{2} c_{p,C} T_{C2}\right) = \frac{1-f_d}{2} P + \left(\frac{UA}{2}\right)_{FC}(T_F - T_{C1}) - \dot{m}_c c_{p,C}(T_{C2} - T_{C1}) \quad (19)$$

The reactivity feedback balance for the model of one fuel node and two coolant nodes is given by Eq. (20) [26].

$$\rho(t) = \rho_{ext} + \alpha_F\left(T_F(t) - T_{F,0}\right) + \frac{\alpha_C}{2}\left(T_{C1}(t) - T_{C1,0}\right) + \frac{\alpha_C}{2}\left(T_{C2}(t) - T_{C2,0}\right) \quad (20)$$

The value of the heat transfer coefficient from the fuel cladding surface (h_s) to the primary coolant is calculated by the Dittus-Boelter correlation. This correlation is shown by Eq. (21) below [12].

$$h_s = \left(0.042\frac{p}{d} - 0.024\right)\frac{k}{D_e} Re^{0.8} Pr^{1/3} \quad (21)$$

Where the pin pitch (p) dan fuel rod diameter (d) are 1.26 cm and 0.95 cm respectively. The Eq. (21) is valid for $0.7 < Pr < 100$; $Re > 10{,}000$; $H/d > 60$.

The UO_2 heat capacity value is obtained based on the heat capacity equation as a function of temperature. ($C_p(T)$). The Eq. (22) is valid for temperatures 298.5 K ≤ T ≤ 3120 K.

$$C_p(T) = 52{,}1743 + 87{,}95t - 84{,}241t^2 + 31{,}542t^3 - 2.6334t^4 - 0{,}7139t^{-2} \quad (22)$$

Where, t=T/1000 [28]. Whereas the water properties are obtained from the International Association for the Properties of Water and Steam Industrial Formulation 1997 (IAPWS-IF97).

RESULTS AND DISCUSSION

Simulation of core dynamics in Labview

Simulation data is collected in automatic mode until the power operation parameters reach a steady state. Parameters recorded include thermal power, inlet moderator temperature, outlet moderator temperature, fuel temperature, cladding temperature, total reactivity, and neutron flux. This automatic mode is used to control the thermal power of the simulator by adjusting the regulating control rod to ensure that the power additions do not exceed a specified value. Figure 6 shows the automatic mode logic in LabVIEW software.

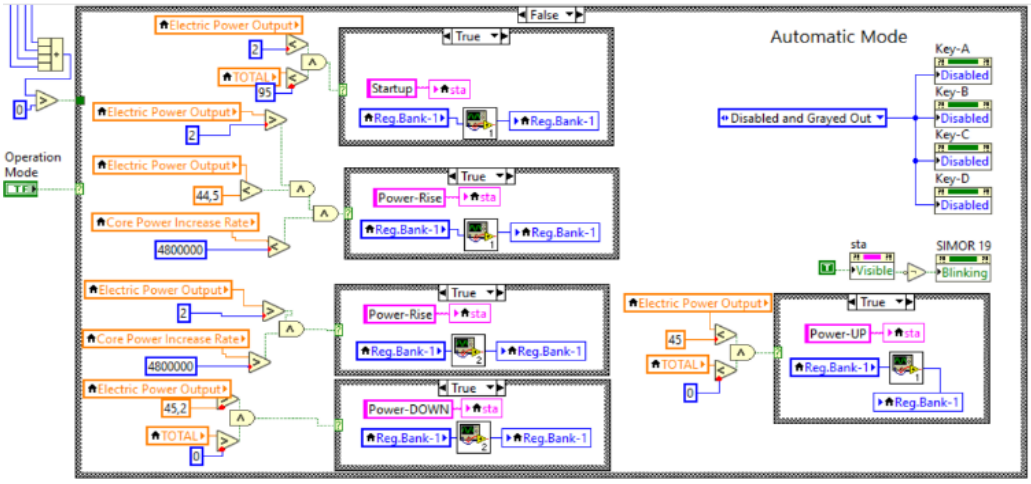

Fig. 6. Automatic mode logic in LabVIEW software.

The collected data are graphed in time series to analyze the dynamics during steady state. Additionally, control rod worth data and temperatures of the fuel and moderator at maximum power are compared with NuScale reactor design certification data to assess the suitability of the developed model.

Control Rod Worth

The control rods in the reactor core contain neutron-absorbing materials. Each control rod can adjust reactor power by providing or reducing reactivity. In the NuScale Reactor, the control rods are divided into four groups: Regulating 1, Regulating 2, Safety 1, and Safety 2. Each group can move simultaneously. The reference control rod worth is defined as the maximum control rod worth for each group at the beginning of the cycle (BOC), Hot Full Power (HFP), and Power Dependent Insertion Limit (PDIL) conditions. The reactivity provided by the control rods under these conditions is crucial for the power maneuvering process. As shown in Table 2 below, the modeled control rod worth is close to the reference values.

Table 2. Control rod worth data.

Control Rod Group	Control Rod Worth	
	Simulation (pcm)	Reference [13] (pcm)
Regulating 1	1361.01	1361
Regulating 2	3577.66	3577.6
Safety 1	4827.58	4827.7
Safety 2	4834.1	4834.3

The control rods move from step 0 to step 225, where step 225 represents the fully inserted position, providing maximum negative reactivity, and step 0 represents the fully withdrawn position, providing minimum negative reactivity. The integral control rod worth for each group is shown in Fig. 7.

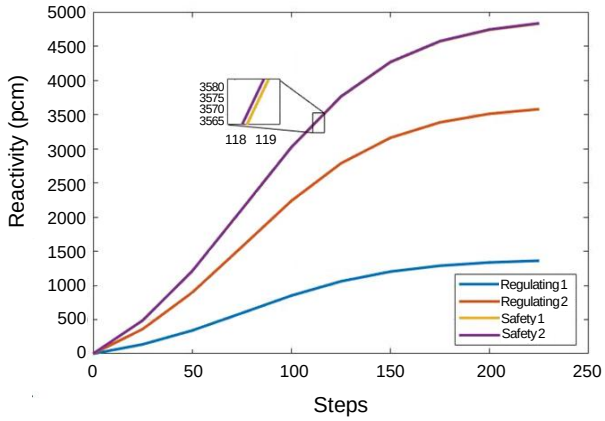

Fig. 7. Integral control rod worth graph.

Neutron calculation

The implementation of the point kinetics equation by solving the inhour equation in LabVIEW is shown in Fig. 8 below. The inputs for the calculation include reactivity value, neutron fraction, decay constant, and initial neutron flux. The value of ω_j is calculated using the Ridder Zero Finder VI Function Block, with the input parameters including reactivity ρ and kinetic parameters such as the decay constant and delayed neutron fraction. Subsequently, ω_j is used to determine A_j via the Eval Single-Variable Scalar VI function block. The values of ω_j and A_j are arranged into arrays, which are inverted using the Reverse 1D Array Function. Finally, these arrays are used in an exponential equation to calculate the neutron flux.

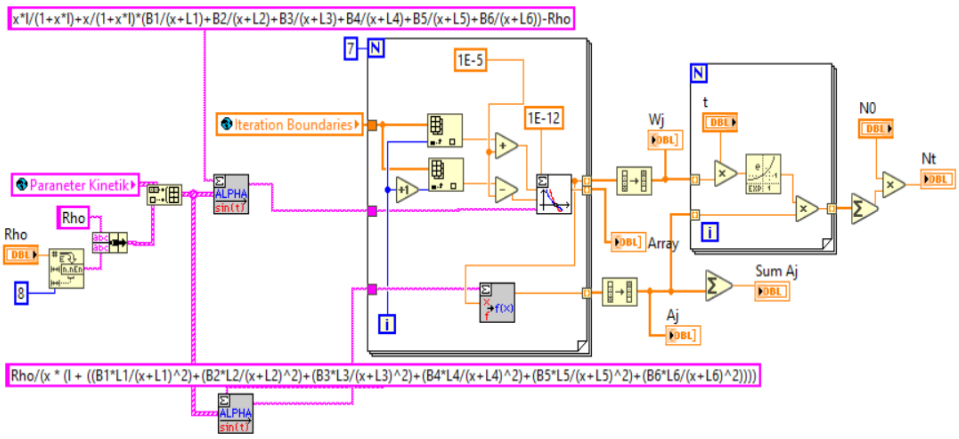

Fig. 8. Implementation of inhour equation in LabVIEW.

Figure 9 shows a graph of thermal power and neutron flux from a simulation run for 2.1 hours in automatic mode. The thermal power reached 160 MWt in approximately 2500s, while the maximum neutron flux was 8.4×10^{13} n/cm^{2}s. The similarity in the shape of the curve for thermal power and neutron flux is due to the thermal power is a direct conversion of neutron flux. At the beginning of full power, the neutron flux experienced significant changes because the moderator temperature had not yet reached its maximum, resulting in negative reactivity provided by the moderator. The control rod aims to maintain the power at 160 MWt. This control process causes significant changes in neutron flux. As shown in Fig. 14, the moderator temperature starts to stabilize after 3700 seconds. Once the moderator temperature reaches a steady state, the neutron flux remains relatively stable.

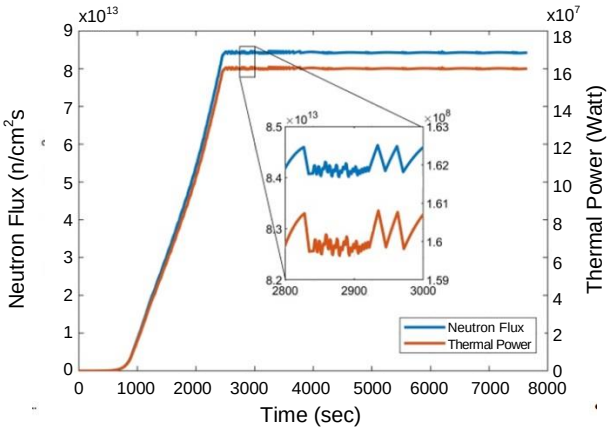

Fig. 9. Thermal power and neutron flux.

Total reactivity during power operation

In the startup condition, the reactivity of the control rod is limited to 95 pcm. Once this value is reached, the control rod position remains fixed. As shown in Fig. 10, the total reactivity is highest during the startup phase. This is due to the Doppler effect, where the moderator and fuel temperatures are at their lowest at the beginning of power operation, providing positive reactivity to the core. As power increases, both the fuel and moderator temperature rise, reducing the total reactivity. The startup condition concludes when the power reaches 2 MWe. Since the secondary loop system is not modeled, the electrical power is calculated by multiplying the thermal power by a factor of 0.28125. At this stage, the Regulating 1 control rod manages the core reactivity to ensure that the power increase rate does not exceed 4.8 MWt/min or 3 %/min.

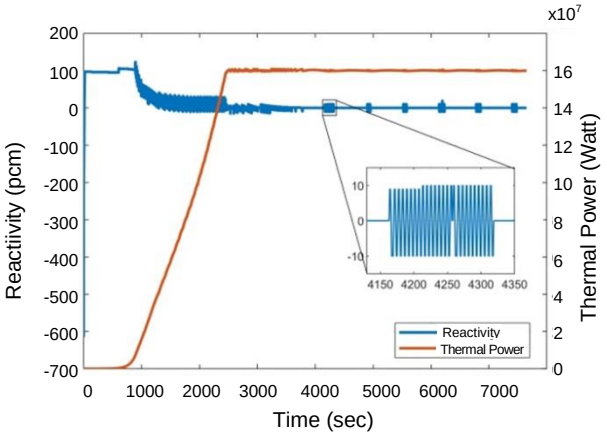

Fig. 10. Total Reactivity during power operation.

Fuel and moderator temperature

The temperature calculations for the cladding and fuel meat are performed using the thermal resistance approach, as described by Eqs. (14)-(16). The temperature of each component varies with the reactor power. Figure 11 shows the fuel temperature calculation in LabVIEW. The four loops on the right are used to illustrate the fuel temperature profile.

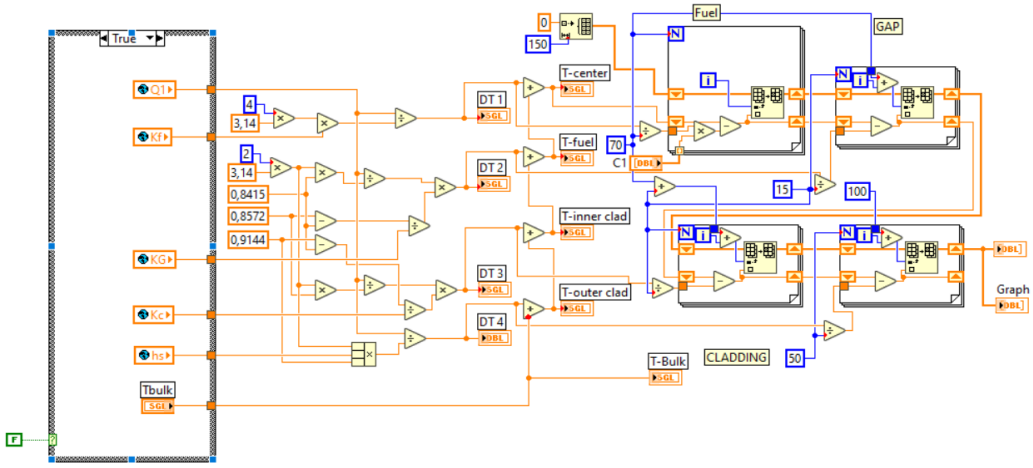

Fig. 11. Fuel Temperature calculation.

The maximum temperature the fuel can reach is 384°C, which then drops to 342°C at the fuel wall. The maximum temperatures for the inner and outer cladding are 328°C and 325°C, respectively. The temperature profile of the fuel is shown in Fig. 12.

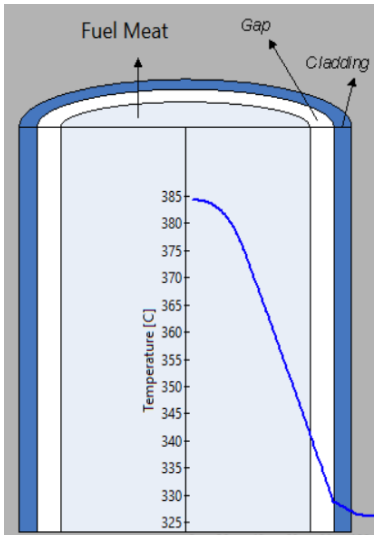

Fig. 12. Fuel temperature profile.

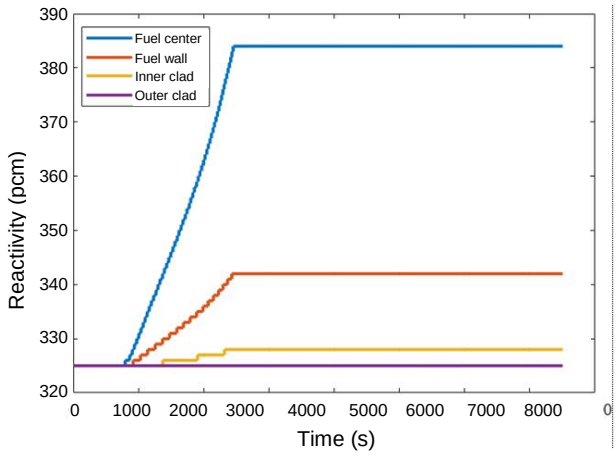

Fig. 13. Fuel temperature.

Figure 13 displays the fuel temperature during power operation. The increase in power significantly affects the fuel temperature, while, the temperatures of the inner and outer cladding are less sensitive to changes in reactor power.

The differential equation for heat transfer from fuel to coolant is solved using 2nd order Runge-Kutta method. Data on the density, viscosity, and thermal conductivity of water are obtained from the IAPWS-IF97-based water and steam table. Curve fitting is then performed on the data to derive a temperature function.

Based on the modeling, the inlet coolant temperature at maximum power is 258 °C, while the temperatures at coolant nodes 1 and 2 are 293 °C and 319 °C, respectively, as shown in Fig. 14. The fuel and moderator temperature data at maximum power were compared with the iPWR-type SMR core design specifications, as shown in Table 3. Although there is a slight difference between modeled and reference temperatures. This discrepancy is due to the selected approaches and model simplification to ensure efficient simulation. With a relatively small error, the simulator can be considered capable of accurately illustrating the dynamics of power operation under normal conditions.

Table 3. Comparison of simulation parameters with SMR design specification.

Parameter	Reference	Simulation
Thermal power (MWt)	160 [13]	160
Core outlet temperature (°C)	319 [13]	319
Core inlet temperature (°C)	262 [13]	258
Fuel temperature (°C)	387 [29]	384

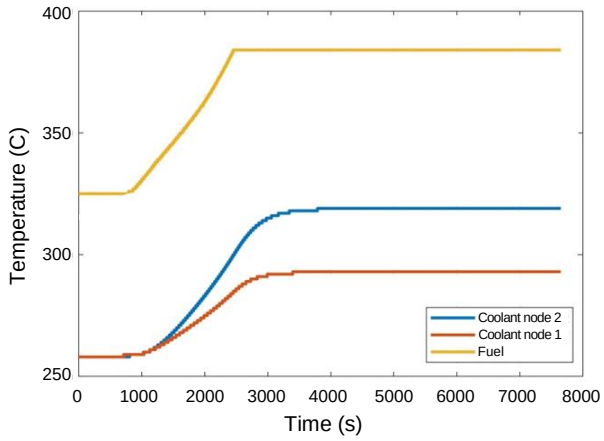

Fig. 14. Fuel and moderator temperature.

Simulator display

Figure 15 displays the simulator interface. The red box highlights a panel with indicator LEDs used during simulator operation. The yellow box features a panel with three tabs, each providing information on core mapping, core thermal hydraulics, and reactor vessel monitoring. The green box contains gauge meters for neutron flux, thermal power, and period, as well as the control rod movement mechanism. The purple box is used to display graphs of core power and reactivity. Finally, the black box includes the SCRAM and operation mode buttons, along with buttons to bring up the popup screen.

Fig. 15. Simulator display.

CONCLUSION

Reactor core modeling for SMR simulator development has been carried out. The core was modeled using the point kinetics method, incorporating reactivity inputs from control rods, fuel temperature, moderator temperature, and xenon poisoning. The performance of the model was assessed by comparing its results with the reactor design certification data. The modeled core is capable of operating up to 160 MWt/45 MWe. The test results for operating parameters at maximum power show good agreement with the SMR reactor design certification data.

NOMENCLATURE

n or $n(t)$	= Neutron density, n/cm^3
β or β_{eff}	= Effective delayed neutron fraction
$C_i(t)$	= Delayed neutron precursor of i-th group
Λ	= Mean generation time, s
ρ	= Reactivity, pcm
λ_i	= Decay constant for delayed neutron precursor of i-th group, s^{-1}
β_i	= Delayed neutron fraction of i-th group
T	= Reactor period, s
P	= Reactor thermal power, Watt
V_r	= Reactor volume, cm^3
Σ_f	= Fission macroscopic cross-section, barn
ϕ	= Neutron flux, n/cm^{2}s
A_j	= Inhour equation coefficients
ω_j	= Inhour equation roots
$\rho(z)$	= control rod reactivity as a step function
$bank_{worth}$	= Total rod worth
z	= Steps
x_0	= 76.053
b	= -36.967
λ_X	= Xenon decay constant, s^{-1}
λ_I	= Iodine decay constant, s^{-1}
γ_X	= Xenon yield
γ_I	= Iodine yield
X	= Xenon concentration
X_0	= Initial xenon concentration
q'	= Heat flux, W/m^2
k_f	= Fuel conductivity, W/m^{o}C
R_g	= Average gap radius, cm
h_g	= effective gap conductance, W/cm^{2o}C
R_c	= Average cladding radius, cm
k_c	= cladding conductivity, W/m^{o}C
δ_c	= cladding thickness, cm
T_{max}	= Maximum fuel temperature, ^{o}C
T_{fo}	= Outer temperature of fuel meat, ^{o}C
T_{ci}	= Inner cladding temperature, ^{o}C
T_{co}	= Outer cladding temperature, ^{o}C
m_F	= Fuel mass, kg
$C_{P,F}$	= Fuel specific heat, J/kg^{o}C
f_d	= Power fraction directly deposited in the fuel
U_{FC} or h	= Heat transfer coefficient from fuel to coolant, W/cm^{2o}C
A_{FC}	= Effective heat transfer area, cm2
T_F	= Fuel temperature, ^{o}C
T_C	= Coolant temperature, ^{o}C
T_{C1}	= Coolant node 1 temperature, ^{o}C
T_{C2}	= Coolant node 2 temperature, ^{o}C
m_C	= Coolant mass, kg
$C_{p,C}$	= Coolant specific heat, J/kg^{o}C
T_{Ci}	= Inlet coolant temperature
$\dot{m}_C$	= Coolant flow rate, kg/s
α	= Reactivity coefficient, pcm/^{o}C
Nu	= Nusselt number
Re	= Reynold number
Pr	= Prandtl number
k	= Thermal conductivity, W/m^{o}C
D_e	= Equivalent hydraulic diameter, m
H	= Active core Height, m

ACKNOWLEDGMENT

We would like to express our gratitude to all individuals and parties who have lent their assistance to this endeavor. The collective effort, whether through discussion, provision of sources, or general support, has played a pivotal role in the successful completion of this work. This work was supported by RIIM funding under Grant No. B-811/II.7.5/FR/6/2022 and 2103/III.2/HK.4.03/7/2022.

AUTHOR CONTRIBUTION

Gilang Septawijaya is the corresponding author, he developed the simulator and wrote the draft manuscript. Dr. Sukarman, Dr. Syaiful Bakhri, and Dr. Muhammad Subekti are co-authors, they helped improve the simulator, revised the draft manuscript, and provided essential data. All authors read and approved the manuscript.

REFERENCES

1. T. Murakami, V. Anbumozhi, Small Modular Reactor (SMR) Deployment: Advantages and Opportunities for ASEAN, ERIA (2022).
2. Dewan Energi Nasional (DEN) (2024). (in Indonesian). https://www.den.go.id/berita/pltn-pertama-indonesia-ditargetkan-beroperasi-tahun-2032. Retrieved in June (2024)
3. C. Zeliang, Y. Mi, A. Tokuhiro *et al.*, Energies **13** (2020) 1.
4. D. Ingersoll and M. Carelli, Handbook: Fundamental of Small Modular Nuclear Reactors, Elsevier (2020).
5. Nuryanti, Suparman, M. Nasrullah *et al.*, Jurnal Pengembangan Eneri Nuklir **17** (2015) 133. (in Indonesian)
6. International Atomic Energy Agency (IAEA), Classification, Selection and Use of Nuclear Power Plant Simulators for Education and Training, TECDOC 1887, Vienna (2019).
7. C. Blackett, M. H. R. Eitrheim, R. Mcdonald *et al.*, Human Performance in Operation of Small Modular Reactors, Honolulu (2022).
8. H. Ardiansyah and M. R. Oktavian, Atom Indones. **47** (2021) 85.
9. Blackett, *Human Factors and Simulation*, in: Proceeding of the 14th International Conference of Applied Human Factor and Economics (AHFE), San Francisco, USA (2023).
10. B. Poudel, K. Joshi, R. Gokaraju, IEEE Trans. Energy Convers. **35** (2020) 977.
11. J. Al-Zain, O. El Hajjaji, T. El Bardouni *et al.*, Moscow Univ. Phys. Bull. **77** (2022) 922.
12. S. E. Arda and K. E. Holbert, Prog. Nucl. Energy **91** (2016) 116.
13. NuScale, Part 02 - Final Safety Analysis Report (Rev. 5) - Part 02 - Tier 02 - Chapter 04 - Reactor - Sections 04.01 - 04.06 (2020).
14. P. Suk, O. Chvála, G.I. Maldonado *et al.*, Nucl. Eng. Des. **371** (2021) 110956.
15. Y. Oka, K. Suzuki, Nuclear Reactor Kinetics and Plant Control, Tokyo (2013).
16. J. Malec, D. Toškan, L. Snoj, Ann. Nucl. Energy **146** (2020) 107630.
17. I. Mahfudin, A. Abimanyu, Syarip, Ganendra **23** (2020) 47. (in Indonesian)
18. W. M. Stacey, Nuclear Reactor Physics, Second Edition, Willey-VCH, Atlanta (2007).
19. A. J. Arul, K. Obaidurrahman, R. R. Prasad *et al.*, Phys. Nucl. React. (2021) 373.
20. M. S. Rahman, M. A. M. Soner, M. M. Rahman *et al.*, Ann. Nucl. Energy **124** (2019) 533.
21. K. Frick and S. Bragg-Sitton, Nucl. Technol. **207** (2021) 521.
22. A. R. M. Iasir and K. D. Hammond, J. Appl Phys **131** (2022) 025105.
23. K. K. Abdulraheem, S. A. Korolev, Z. Laidani, Ann. Nucl. Energy **156** (2021) 108193.
24. K. K. Abdulraheem and S. A. Korolev, Ann. Nucl. Energy **158** (2021) 108288.
25. N. E. Todreas, M. S. Kazimi, Nuclear System: Thermal Hydraulic Fundamentals **1** (2011).
26. B. Puchalski, T. A. Rutkowski, K. Duzinkiewicz, Nucl. Eng. Des.**322** (2017) 444.
27. M. El-Sefy, M. Ezzeldin, W. El-Dakhakhni *et al.*, Nucl. Eng. Technol. **51** (2019) 1540.
28. M. Reymond, J. Sercombe, L. Gallais *et al.*, J. Nucl. Mater. **557** (2021) 153220.
29. Z. Rahnama and G. R. Ansarifar, Ann. Nucl. Energy **161** (2021) 108375.